

# HEART: Achieving Timely Multi-Model Training for Vehicle-Edge-Cloud-Integrated Hierarchical Federated Learning

Xiaohong Yang, Minghui Liwang, *Member, IEEE*, Xianbin Wang, *Fellow, IEEE*, Zhipeng Cheng, Seyyedali Hosseinalipour, *Member, IEEE*, Huaiyu Dai, *Fellow, IEEE*, Zhenzhen Jiao

**Abstract**—The rapid growth of AI-enabled Internet of Vehicles (IoV) calls for efficient machine learning (ML) solutions that can handle high vehicular mobility and decentralized data. This has motivated the emergence of Hierarchical Federated Learning over vehicle-edge-cloud architectures (VEC-HFL). Nevertheless, one aspect which is underexplored in the literature on VEC-HFL is that vehicles often need to execute multiple ML tasks simultaneously, where this multi-model training environment introduces crucial challenges. First, improper aggregation rules can lead to model obsolescence and prolonged training times. Second, vehicular mobility may result in inefficient data utilization by preventing the vehicles from returning their models to the network edge. Third, achieving a balanced resource allocation across diverse tasks becomes of paramount importance as it majorly affects the effectiveness of collaborative training. We take one of the first steps towards addressing these challenges via proposing a framework for multi-model training in dynamic VEC-HFL with the goal of minimizing global training latency while ensuring balanced training across various tasks—a problem that turns out to be NP-hard. To facilitate timely model training, we introduce a hybrid synchronous-asynchronous aggregation rule. Building on this, we present a novel method called Hybrid Evolutionary And gReedy allocaTion (HEART). The framework operates in two stages: first, it achieves balanced task scheduling through a hybrid heuristic approach that combines improved Particle Swarm Optimization (PSO) and Genetic Algorithms (GA); second, it employs a low-complexity greedy algorithm to determine the training priority of assigned tasks on vehicles. Experiments on real-world datasets demonstrate the superiority of HEART over existing methods.

**Index Terms**—Hierarchical federated learning, Internet of Vehicles, Multi-model training, Distributed machine learning.

## I. INTRODUCTION

THE rapid advancement of Artificial Intelligence (AI), communication and computing technologies, as well as evolving vehicle design requirements have led to the integration of Machine Learning (ML)-driven applications within the Internet of Vehicles (IoV) [1], [2], aiming to enhance vehicular services and driving experiences. However, the distributed

Xiaohong Yang is with the School of Informatics, Xiamen University, Fujian, China. Minghui Liwang is with the Department of Control Science and Engineering, the National Key Laboratory of Autonomous Intelligent Unmanned Systems, and also with Frontiers Science Center for Intelligent Autonomous Systems, Ministry of Education, Tongji University, Shanghai, China. Xianbin Wang is with the Department of Electrical and Computer Engineering, Western University, Ontario, Canada. Zhipeng Cheng is with the School of Future Science and Engineering, Soochow University, Suzhou, China. Seyyedali Hosseinalipour is with the department of Electrical Engineering, University at Buffalo-SUNY, Buffalo, NY USA. Huaiyu Dai is with the Department of Electrical and Computer Engineering, NC State University, Raleigh, NC, USA. Zhenzhen Jiao is with the iF-Labs, Beijing Teleinfo Technology Company, Ltd, CAACT, Beijing, China.

nature of data generated across the IoV and the high mobility of vehicles introduce significant challenges to the efficient utilization of IoV data for ML training purposes. This is due to the fact that conventional ML training methods often rely on centralized procedures that entail transferring data from all data-generating units (e.g., vehicles) to a single location (e.g., a cloud server). This approach results in high latency, increased network traffic congestion, and raises privacy concerns due to the exposure of raw data. Federated Learning (FL) has emerged as an innovative distributed ML framework that addresses these issues by pushing model training to the data-generating units themselves, thereby preserving data privacy and reducing communication overhead [3]. Nevertheless, in dynamic vehicular environments, FL still suffers from low communication efficiency and frequent communication failures [4]–[6] due to the high mobility of vehicles and unstable network connections. To overcome these challenges, Hierarchical Federated Learning (HFL) has been proposed as a multi-layer extension of FL [7]. HFL introduces intermediate aggregators (e.g., edge servers) between the vehicles and the cloud server, helping to balance the trade-off between communication efficiency and computational overhead. This hierarchical approach enhances the robustness and efficiency of the learning process, making HFL a promising solution for efficient ML training and execution in IoV systems.

## A. Integration of FL and HFL into the IoV Ecosystem

Recent integrations of conventional FL and HFL over IoV systems predominantly emphasize single-task/model FL [8]–[10], where all vehicles are engaged in training a single ML model. However, in real-world vehicular networks, vehicles often need to execute multiple ML tasks simultaneously, such as object detection for autonomous driving, traffic prediction for route optimization, and driver behavior analysis for safety enhancements. This necessitates the use of multi-model training approaches that can handle diverse ML models concurrently. Despite its promising potential, there exists very limited literature addressing multi-model FL over wireless networks [11], [12], and these works often rely on conventional FL training methods, which face significant communication overhead. Consequently, reducing communication costs while accelerating the overall multi-model training process is a primary concern that demands critical attention for both IoV systems and wireless networks more broadly.

Some early efforts have been dedicated to address these concerns, focusing on the conventional FL architecture. For instance, recent studies have considered the unique characteristics of diverse ML models by leveraging vehicle-side resources to reduce the required number of global iterations, thereby ensuring timely and efficient model training [13], [14]. In these approaches, local models are collectively transmitted only once when their training is finalized on the vehicles, effectively minimizing the frequency of communication with the global aggregator, e.g., a cloud server [6]. Additionally, some research highlights the importance of selecting appropriate clients for training and effectively aggregating results from various tasks in FL [15]. While these contributions have advanced the new field, they often overlook the impact of balanced scheduling of ML tasks on global model convergence when handling multiple tasks with a HFL over dynamic IoV systems. In such systems, risks may arise due to model obsolescence if the trained models are not promptly aggregated upon completion [5]. Further, improper prioritization of task training on vehicles can lead to prolonged waiting times for model aggregation, further exacerbating potential model obsolescence.

### B. Motivation and Overview of Our Methodology

This work is among the first in the literature to address the multi-model training within VEC-HFL. In our problem of interest, vehicles serve as training clients, multiple edge servers (ESs) act as middle-layer aggregators, and a cloud server (CS) functions as the global aggregator. We first note that a key challenge in facilitating multi-model training is mitigating model obsolescence risks while enhancing the utilization of distributed and dynamic training data from vehicles. In particular, we observe that traditional model aggregation methods in FL and HFL are either synchronous or asynchronous. Synchronous aggregation waits for all clients to upload their models to maintain consistency, but this can introduce significant delays and increase the risk of model obsolescence. Conversely, asynchronous aggregation initiates the aggregation process as soon as a subset of clients uploads their models, effectively reducing latency. However, this method may suffer from model instability and struggle to fully utilize data from all participating clients, potentially impacting the convergence speed of the global model. To address these challenges, we introduce a *hybrid synchronous-asynchronous aggregation rule for VEC-HFL*. This rule operates on a per-task basis: at the edge layer, each ES performs an aggregation only after receiving all local models of a specific task from vehicles (synchronous approach), while at the cloud layer, the CS conducts a global aggregation after obtaining a subset of the corresponding ES models (asynchronous approach). This hybrid approach leverages the advantages of both synchronous and asynchronous methods. By synchronously aggregating at the edge layer, we ensure model consistency and fully utilize the local training data from all participating vehicles, enhancing model accuracy and convergence speed. Simultaneously, the asynchronous aggregation at the cloud layer reduces overall latency by not waiting for all ESs, which can have different delays of model aggregation based on the distribution of vehicles covered by them and their channel conditions, to report their models, thereby mitigating delays and the risk of model

obsolescence. This combination provides a natural solution that balances the trade-offs between timeliness and model quality, making it particularly suitable for dynamic IoV environments where both factors are critical.

Building on this novel hybrid aggregation rule, we then target minimizing the global time/latency costs while ensuring balanced training across diverse ML tasks over resource-limited vehicles. We formulate this problem as a min-max optimization that turns out to be NP-hard, making the obtaining of its solution challenging in dynamic IoV systems. To tackle this problem, we propose a stagewise solution called the *Hybrid Evolutionary And gReedy allocation method (HEART)*. In *Stage 1* of HEART, we optimize the assignment between model training tasks and heterogeneous resource-limited moving vehicles. To this end, leveraging the strong global search capabilities and computational efficiency of Particle Swarm Optimization (PSO) and Genetic Algorithms (GA), we develop an efficient combination of improved PSO and GA to achieve or closely approximate the optimal and balanced task assignment solution. In *Stage 2* of HEART, we coordinate the training sequence/rank of assigned tasks on each selected vehicle to accelerate decision-making by designing a greedy-based task ranking optimization method.

### C. Summary of Contributions

Our major contributions can be summarized as follows:

- *Hybrid Synchronous-Asynchronous Aggregation Rule for Multi-Model Training in VEC-HFL*: We introduce a novel aggregation rule tailored for VEC-HFL. This hybrid approach performs synchronous aggregation at the ES and asynchronous aggregation at the CS. By doing so, it effectively leverages the rich data generated by vehicles while significantly mitigating the adverse effects of model obsolescence, thereby enhancing the overall timeliness of the training process across ML tasks.
- *Efficient Two-Stage Optimization Method, HEART, to Minimize Global Time Cost*: Addressing the NP-hard nature of minimizing the overall time cost in the VEC-HFL process, we develop an efficient two-stage optimization method named HEART. In Stage 1, we optimize task scheduling for vehicles by designing a hybrid Particle Swarm Optimization-Genetic Algorithm (PSO-GA), which combines the global search capabilities of PSO with the robust convergence properties of GA. In Stage 2, we optimize the task training sequence on the vehicle side by introducing a low-complexity greedy algorithm, which sequentially assigns tasks to maximize overlap and minimize uploading time. This two-pronged approach ensures both effective task distribution and efficient training sequence/rank planning, benefiting from a low computational complexity while maintaining high performance.
- *Superior Performance Demonstration through Extensive Simulations on Real-World Datasets*: We conduct comprehensive simulations using real-world datasets to evaluate the performance of HEART. The results demonstrate its superior performance in terms of time efficiency and the overall communication costs compared to baseline methods. These findings highlight the effectiveness of HEART in dynamic IoV systems, showcasing its potential for practical deployment and scalability in real-world scenarios.

The remaining of this paper is structured as follows. Section II provides relevant background and description. Section III presents the framework for multi-model task training and scheduling in VEC-HFL. Section IV provides problem formulation and solution description. Section V provides simulation results, and Section VI concludes this work and outlines interesting future work directions.

## II. BACKGROUND AND PRELIMINARIES

The VEC-HFL architecture of our interest (see Fig. 1) comprises one CS as the global aggregator, multiple ESs as middle-layer aggregators, and multiple vehicles as model training clients moving between ESs. We collect the ESs via the set  $\mathcal{M} = \{1, \dots, M\}$ , where each ES  $m \in \mathcal{M}$  has a certain communication coverage. Also, we denote the set of vehicles in the IoV system by  $\mathcal{N} = \{1, \dots, N\}$ , where each vehicle  $n \in \mathcal{N}$  is assumed to be located inside the considered IoV region during the training process, moving between the ESs. Moreover, we denote the set of all ML tasks in the system by  $\mathcal{J} = \{1, \dots, J\}$ , which are expected to be scheduled and trained/executed over moving vehicles.

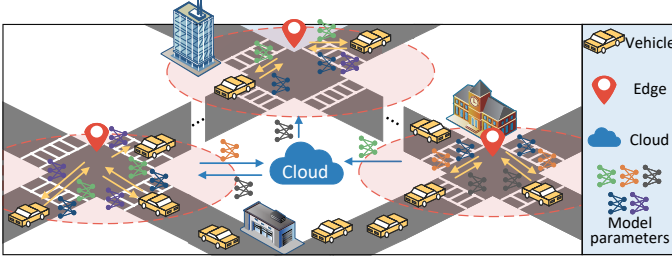


Fig. 1: A schematic of multi-model training over VEC-HFL.

To enhance data utilization and mitigate model obsolescence, we introduce a hybrid synchronous- asynchronous aggregation rule for VEC-HFL as illustrated in Fig. 2. Presuming a specific task/model training rank across the vehicles (further concer- tized in Section III and optimized in Section IV), once vehicle  $n$  completes the local training of a task  $j \in \mathcal{J}$ , it transmits the local model to its associated ES, and then proceeds to training the next task according to the task ranking. In this framework, for each task  $j$ , an ES waits for the reception of local models of all the vehicles in its coverage who train this task before conducting a local model aggregation for this task. Once the models for task  $j$  are aggregated at each ES, the ES broadcasts the updated edge model back to its associated vehicle to prompt the start of the next local training round at the vehicles. Differently, the CS employs an asynchronous aggregation rule where once it receives a subset of edge models (e.g., from  $Q^{(j)}$  ESs) for task  $j$ , it performs global aggregation and broadcasts the updated model to the ESs.

Subsequently, the processes taken place in VEC-HFL can be divided into *local iterations* (i.e., local ML training using stochastic gradient descent), *edge iterations* (i.e., model transfer from the vehicles to the ESs followed by model aggregation), and *global iterations* (i.e., model transfer from a subset of ESs to the CS followed by model aggregations), where we use notation  $h$ ,  $k$  and  $g$  to index them, respectively. Besides, for different task (e.g., task  $j$ ), we also set corresponding maximum number of local iteration and edge iterations to be  $H^{(j)}$  and  $K^{(j)}$ , which implies  $h \in \{1, \dots, H^{(j)}\}$  and

$k \in \{1, \dots, K^{(j)}\}$ . We assume that the training of each task  $j$  starts with broadcasting a unified global model  $\varpi_{[0]}^{(j)}$  across all the ESs and vehicles and further assume that each task  $j$  continues its global iterations until its global model satisfies its convergence condition. Consequently, the maximum number of global iterations  $g$  is not predetermined. Next, we provide a mathematical formalization of the VEC-HFL architecture.

For each task  $j$ , we model the dataset of the  $n^{\text{th}}$  vehicle within the coverage of ES  $m$  as  $\mathcal{D}_{m,n}^{(j)} = \{(x_i, y_i) : 1 \leq i \leq |\mathcal{D}_{m,n}^{(j)}|\}$ , where  $x_i$  and  $y_i$  describe the feature vector and the label of the  $i^{\text{th}}$  data point and  $|\mathcal{D}_{m,n}^{(j)}|$  represents the size of the dataset. Accordingly, the loss function of task  $j$  at this vehicle is given by

$$L_{m,n}^{(j)} \left( \omega_{m,n;[g,k,h]}^{(j)} \right) = \sum_{i=1}^{|\mathcal{D}_{m,n}^{(j)}|} l_i^{(j)} \left( \omega_{m,n;[g,k,h]}^{(j)} \right), \quad (1)$$

where  $l_i^{(j)} \left( \omega_{m,n;[g,k,h]}^{(j)} \right)$  denotes the loss function for the  $i^{\text{th}}$  data point given the instantaneous local model parameters  $\omega_{m,n;[g,k,h]}^{(j)}$  for the  $n^{\text{th}}$  vehicle covered by ES  $m$  during the  $h^{\text{th}}$  local iteration of the  $k^{\text{th}}$  edge iteration of global iteration  $g$ . In particular, the update process of the instantaneous local model on this vehicle is carried out using stochastic gradient descent (SGD) iterations as follows ( $h \in \{1, \dots, H^{(j)}\}$ ):

$$\omega_{m,n;[g,k,h]}^{(j)} = \omega_{m,n;[g,k,h-1]}^{(j)} - \eta^{(j)} \nabla L_{m,n}^{(j)} \left( \omega_{m,n;[g,k,h-1]}^{(j)}, \mathcal{B}_{m,n;[g,k,h]}^{(j)} \right), \quad (2)$$

where  $\eta^{(j)}$  is the learning rate, and  $\mathcal{B}_{m,n;[g,k,h]}^{(j)}$  is a mini-batch of data sampled randomly from the local dataset  $\mathcal{D}_{m,n}^{(j)}$ . The local model of the edge iteration  $k$  for each global iteration  $g$  is initialized with  $w_{m,n;[g,k,0]}^{(j)} = \tilde{w}_{m;[g,k-1]}^{(j)}$  which is the latent model received from the edge. Also, the latest local model  $w_{m,n;[g,k,H^{(j)}]}^{(j)}$  is sent to the ES and used to obtain the next edge model as discussed below.

Considering the  $k^{\text{th}}$  edge iteration of global iteration  $g$  for an ES  $m$ , we denote the set of vehicles under its coverage who also train task  $j$  as  $\mathcal{N}_{m;[g,k]}^{(j)}$ . Letting  $\tilde{\omega}_{m;[g,k]}^{(j)}$  represent the edge model for task  $j$  at the  $k^{\text{th}}$  edge iteration of global iteration  $g$ , its update can be expressed as follows:

$$\tilde{\omega}_{m;[g,k]}^{(j)} = \sum_{n \in \mathcal{N}_{m;[g,k]}^{(j)}} \frac{|\mathcal{D}_{m,n}^{(j)}|}{|\tilde{\mathcal{D}}_{m;[g,k]}^{(j)}|} \omega_{m,n;[g,k,H^{(j)}]}^{(j)}, \quad (3)$$

where  $\tilde{\mathcal{D}}_{m;[g,k]}^{(j)} = \bigcup_{n \in \mathcal{N}_{m;[g,k]}^{(j)}} \mathcal{D}_{m,n}^{(j)}$ , and  $|\tilde{\mathcal{D}}_{m;[g,k]}^{(j)}|$  represents the overall data volume for task  $j$  during the  $k^{\text{th}}$  edge iteration possessed by the vehicles covered by ES  $m$ . The latest edge model  $\tilde{\omega}_{m;[g,K^{(j)}]}^{(j)}$  is sent to the CS and used to obtain the next global model as discussed below.

For each  $j \in \mathcal{J}$ , once the CS receives a predetermined number of edge models (i.e.,  $Q^{(j)}$ ), it performs the global aggregation. Let  $\mathcal{M}_g^{(j)}$ , where  $|\mathcal{M}_g^{(j)}| = Q^{(j)}$ , represent the set of ESs who deliver the edge model of task  $j$  to the CS at

the  $g^{\text{th}}$  global aggregation. The update process of global model for task  $j$  is as follows:

$$\varpi_{[g]}^{(j)} = \alpha^{(j)} \varpi_{[g-1]}^{(j)} + (1 - \alpha^{(j)}) \sum_{m \in \mathcal{M}_g^{(j)}} \frac{|\tilde{\mathcal{D}}_{m;[g,K^{(j)}]}^{(j)}|}{|\tilde{\mathcal{D}}_{[g]}^{(j)}|} \tilde{\omega}_{m;[g,K^{(j)}]}^{(j)}, \quad (4)$$

where  $\alpha^{(j)}$  represents the weighting coefficient between the current global model and the updated edge models received from the ESs.  $\tilde{\mathcal{D}}_{[g]}^{(j)} = \cup_{m \in \mathcal{M}_g^{(j)}} \tilde{\mathcal{D}}_{m;[g,K^{(j)}]}^{(j)}$ , and  $|\tilde{\mathcal{D}}_{[g]}^{(j)}|$  represents the overall number of data points involved in training task  $j$  during the  $g^{\text{th}}$  global aggregation. The global model  $\varpi_{[g]}^{(j)}$  is then sent back to these ESs, which relay it back to their covered vehicles to synchronize their local models and start the next round of local training. We consider that the global iterations for each task  $j$  ends at iteration  $g$  when its following convergence criterion

$$\|\varpi_{[g]}^{(j)} - \varpi_{[g-1]}^{(j)}\| \leq \beta^{(j)}, \quad (5)$$

where  $\|\cdot\|$  represents the Euclidean 2-norm, and  $\beta^{(j)}$  represents a small positive value used to control the convergence criterion. Alg. 1 provides an overview of our designed hybrid synchronous-asynchronous aggregation rule for VEC-HFL.

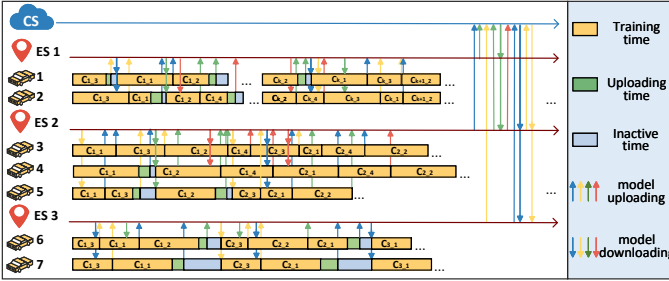


Fig. 2: A schematic of multi-task scheduling and training VEC-HFL architecture of our interest.

### III. MULTI-TASK SCHEDULING OVER VEC-HFL ARCHITECTURE

In this section, to better analyze the time cost of the proposed VEC-HFL architecture, we first analyze the local and edge iterations, deriving the local training time for vehicles and the time required for ESs to complete an entire edge iteration. Then, we provide an analysis for the global iteration.

#### A. Modeling the Time Overhead of Local and Edge Iterations

The time consumed to perform one local training round (i.e., one SGD iteration) at the  $n^{\text{th}}$  vehicle covered by ES  $m$  for task  $j$  can be calculated as follows:

$$t_{m,n;[g,k,h]}^{(j)} = \frac{|\mathcal{B}_{m,n;[g,k,h]}^{(j)}| c_{m,n}^{(j)}}{f_{m,n}^{(j)}} + b_{m,n}^{(j)}, \quad (6)$$

where  $c_{m,n}^{(j)}$  represents the number of cycles that it takes to process one data point of task  $j$ ,  $f_{m,n}^{(j)}$  denotes the allocated CPU clock frequency of the vehicle to conduct ML training for task  $j$ , and  $|\mathcal{B}_{m,n;[g,k,h]}^{(j)}|$  is the number of data points contained in the mini-batch of SGD. Moreover,  $b_{m,n}^{(j)}$  is a constant value,

#### Algorithm 1: Overview of the VEC-HFL of our interest

```

Input :  $H^{(j)}, K^{(j)}, \eta^{(j)}$ ;
Output: Global model  $\varpi_{[g]}^{(j)}$ ;
1 Initialization :  $w_{m,n}^{(j)} = \varpi_{[0]}^{(j)}$ ;
2 if for task  $j$ , where  $j \in \mathcal{J}$ , the global model parameter changes does not satisfy (5) then
3   Edge process: // running at each ES
4   foreach  $m \in \mathcal{M}$  in parallel do
5     for  $k = \{1, 2, \dots, K^{(j)}\}$  do
6       Vehicle process: //  $\bar{x}_{m,n;[g]}$  obtained from Alg. 2
7       foreach  $n \in \mathcal{N}$  in parallel do
8         for  $j \in \{\bar{x}_{m,n;[g]} = 1\}$  in turn do
9           Synchronize the local model based on
10           edge model:  $w_{m,n;[g,k,0]}^{(j)} \leftarrow \tilde{w}_{m;[g,k-1]}^{(j)}$ 
11           vehicle  $n$  undergoes local training in
12           sequence based on the task training
13           rank obtained from Alg. 3
14           for  $h = \{1, 2, \dots, H^{(j)}\}$  do
15             Update local model based on (2),
16             and after training, send the final
17             local model  $\omega_{m,n;[g,k,H^{(j)}]}^{(j)}$  to ES
18       if models received from all  $n \in \mathcal{N}_{m;[g,k]}^{(j)}$  then
19         Update edge model  $\tilde{\omega}_{m;[g,k]}^{(j)}$  based on (3)
20     if the global model parameter changes satisfy (5) then
21          $\mathcal{J} \leftarrow \mathcal{J} \setminus \{j\}$ 

```

representing the migration time of the model between the CPU and GPU, or instantiating the model parameters. Harder tasks (e.g., those that use deeper neural networks) are often associated with larger values of  $c_{m,n}^{(j)}$  and  $b_{m,n}^{(j)}$ .

We model the configuration of task processing (i.e., task-to-vehicle assignment) via a binary indicator variable  $\bar{x}_{m,n;[g]}$ :  $\bar{x}_{m,n;[g]}^{(j)} = 1$  indicates that task  $j$  is processed on the  $n^{\text{th}}$  vehicle of ES  $m$  during the  $g^{\text{th}}$  global iteration; and  $\bar{x}_{m,n;[g]}^{(j)} = 0$  otherwise. Additionally, since the ESs employ a synchronous aggregation rule for each task, when the task sequence of vehicles (i.e., the order in which the vehicles execute their local tasks) within the ES coverage exhibit a higher degree of overlap, the local models of all tasks can be aggregated at shorter intervals to mitigate the effects of model obsolescence. Furthermore, in the dynamic IoV channels considered in this work, uploading local models at optimal times during each edge iteration, which can be achieved through optimizing the task sequence of vehicles, can significantly reduce communication latency and global communication costs. For instance, uploading tasks with larger model parameters when vehicles are closer to the ES dramatically decreases both model upload time and communication delays compared to uploading when

vehicles are farther away.

To formally describe this process, we introduce  $\lambda_{m,n;[g,k]}$  to represent the training sequence of tasks on the  $n^{\text{th}}$  vehicle covered by ES  $m$  during the  $k^{\text{th}}$  edge iteration of global iteration  $g$ . For example, if this vehicle is assigned tasks 1, 3, and 4, then the training sequence  $\lambda_{m,n;[g,k]}$  is [4, 1, 3]. We further use  $\mathcal{I}(\lambda_{m,n;[g]})$  to denote the position of task  $j$  on the  $n^{\text{th}}$  vehicle within the coverage of ES  $m$ . Continuing the previous example, if  $\lambda_{m,n;[g,k]} = [4, 1, 3]$ , then  $\mathcal{I}(\lambda_{m,n;[g]}) = 2$ . This notation helps model the completion time for each task during edge iterations, which in turn provides a tractable framework to address the aforementioned challenges by optimizing the task training sequence  $\lambda_{m,n;[g,k]}$  across various vehicles. Below, we integrate task training sequence in modeling the task completion time and will later provide the details of the optimization of the task training sequence in Section IV.

Due to the complexities involved in modeling the timeline of the processes that take place at each vehicle in our hybrid synchronous-asynchronous aggregation rule, we divide the time span dedicated to conducting local iterations of a vehicle into two parts: *task-training time* and *non-task-training time*. For the former, the task-training time of the  $n^{\text{th}}$  vehicle covered by ES  $m$  to complete a task (e.g., task  $j$ ) during the  $k^{\text{th}}$  edge iteration of the  $g^{\text{th}}$  global iteration can be calculated by considering the number of local iterations ( $H^{(j)}$ ), and the time consumed by each local training round (i.e.,  $t_{m,n;[g,k,h]}^{(j)}$  given by (6)), which can be defined as

$$t_{m,n;[g,k]}^{Cmp,(j)} = \sum_{h=1}^{H^{(j)}} t_{m,n;[g,k,h]}^{(j)}. \quad (7)$$

The non-task-training time primarily consists of (i) the local model upload time and (ii) any idle period from the completion of one task's local iteration to the start of the next<sup>1</sup>. However, modeling this time needs careful considerations because, during the  $g^{\text{th}}$  global iteration, vehicles immediately transmit their local models to the associated ES once they finish training, and thus two scenarios may arise:

- **Case (i): Immediate local execution.** If a vehicle receives the edge model for the next task in its training sequence before completing its current one, it can begin the new local iterations for the next task right away. In this case, since the local training of the next task and model transmission of the finished task occur concurrently, both the upload time of the completed task and the potential idle time can be effectively neglected.

- **Case (ii): Delayed local execution.** If the edge model of the next task in the training sequence of a vehicle is available (i.e., not yet received from the ES) once the current task finishes, the vehicle will experience a nonzero non-task-training time. This includes the upload time of the finished model plus any idle time until the next task is broadcasted and received at the vehicle.

Fig. 2 illustrates the above cases using four training tasks, seven vehicles, and three ESs. Colored arrows (blue, green, yellow, red) represent the uploading and broadcasting processes for tasks 1–4, while  $C_{i,j}$  denotes the  $j^{\text{th}}$  task in the  $i^{\text{th}}$  edge iteration of a global iteration. For example,  $C_{1,2}$  indicates the second task in the first edge iteration. In this figure, Vehicle 1 first completes Task 3 but has no immediate follow-up task to process (i.e., *case (ii)*), so it remains idle until Task 1 is broadcasted by the ES. By contrast, Vehicle 2 receives Task 1 before it finishes Task 3 (i.e., *case (i)*), so it transitions to processing Task 1 without any idle times. In this figure, after collecting two edge models from ESs, the CS performs a global aggregation and re-broadcasts the updated global model to the ESs (see the arrows from the ESs to the CS and from the CS to the ESs on the right side of Fig. 2).

Next, we provide a more formal description of the non-task-training time process. Firstly, the upload time of task  $j$  of the  $n^{\text{th}}$  vehicle covered by ES  $m$  during the  $k^{\text{th}}$  edge iteration of the  $g^{\text{th}}$  global iteration can be expressed by

$$t_{m,n;[g,k]}^{V2E,(j)} = I_{m,n}^{V2E,(j)} / r_{m,n;[g,k]}^{V2E}, \quad (8)$$

where  $r_{m,n;[g,k]}^{V2E}$  represents the vehicle-to-edge data rate of vehicle  $n$  under the coverage of ES  $m$  during the  $k^{\text{th}}$  edge iteration, which is related to the distance between the vehicle and ES and the channel conditions [17]. Besides, the size of the local model (in bits) is denoted by  $I_{m,n}^{V2E,(j)}$ .

Let  $t_{m,n;[g,k]}^{inact,(j)}$  denote the inactive time of the  $n^{\text{th}}$  vehicle covered by ES  $m$  after completing its local iteration at edge iteration  $k$  of global aggregation  $g$ . It can be observed that this inactive time is a function of the completion time of edge iteration  $k-1$  within global aggregation  $g$  for a task  $j$ , which we denote it by  $t_{m,n;[g,k-1]}^{end,(j)}$ . Mathematically, we obtain this inactive time as follows:

$$t_{m,n;[g,k]}^{inact,(j)} = \max \left\{ \underbrace{\max_{n' \in \mathcal{N}_{m,g}^{(j)}} \left\{ t_{m,n';[g,k-1]}^{end,(j)} \right\}}_{(a)} - \underbrace{\overbrace{t_{m,n;[g,k]}^{end,(j')}}_{(b)}, 0} \right\}, \quad (9)$$

where term (a) represents the time where all the other vehicles send their local models of task  $j$  to ES  $m$  at the  $(k-1)^{\text{th}}$  edge iteration, which creates the updated edge model for starting the next edge iteration (i.e., the  $k^{\text{th}}$  within the global iteration  $g$ ), and (b) indicates the time that vehicle  $n$  will start processing task  $j$  during the  $k^{\text{th}}$  edge iteration in global iteration  $g$ . We will later obtain  $t_{m,n;[g,k]}^{end,(j)}$  as a function of  $t_{m,n;[g,k]}^{inact,(j)}$  in (12), which combined with (9) forms a recursive expression between these two quantities.

Subsequently, the non-task training time of the  $n^{\text{th}}$  vehicle covered by ES  $m$  is given by

$$t_{m,n;[g,k]}^{Ntt,(j)} = \begin{cases} 0 & \text{if case (i)} \\ t_{m,n;[g,k]}^{V2E,(j)} + t_{m,n;[g,k]}^{inact,(j)} & \text{if case (ii)} \end{cases}, \quad (10)$$

Therefore, for the  $n^{\text{th}}$  vehicle covered by ES  $m$ , the time required to complete location iterations for task  $j$  in the  $k^{\text{th}}$  edge iteration of global iteration  $g$  can be expressed as

$$t_{m,n;[g,k]}^{(j)} = t_{m,n;[g,k]}^{Cmp,(j)} + t_{m,n;[g,k]}^{Ntt,(j)}. \quad (11)$$

<sup>1</sup>We have disregarded the communication delay of the downlink between ESs-to-vehicles and CS-to-ESs, due to the strong broadcasting capabilities of ESs and CS – similar to [14], [16].

Since the ESs utilize synchronous aggregation rule, it needs to wait for all vehicles assigned to the task to upload their local models before performing edge aggregation. Nevertheless, different vehicles have different training sequences for tasks, and their training and uploading times are also different. Thus, the completion of edge iteration  $k$  of global aggregation  $g$  for a task  $j$  at the  $n^{\text{th}}$  vehicle covered by ES  $m$  is a function of the execution times of the tasks that have lower execution rank as compared to this task (i.e., get processed before task  $j$ ); mathematically, we have

$$t_{m,n;[g,k]}^{\text{end},\langle j \rangle} = \sum_{j': \mathcal{I}(\lambda_{m,n;[g]}^{\langle j' \rangle}) \leq \mathcal{I}(\lambda_{m,n;[g]}^{\langle j \rangle})} t_{m,n;[g,k]}^{\langle j' \rangle} \bar{x}_{m,n;[g]}^{\langle j' \rangle}, \quad j \in \mathcal{J}, \quad (12)$$

where the summation is taken over all the tasks that get executed before task  $j$ , where the execution time of task  $j$  is included as well. Then, combined with the synchronous aggregation rule, the overall time cost/overhead of execution of task training for task  $j$  at ES  $m$ , which is dictated by the last vehicle that uploads its model to the ES, at the end of edge iteration  $k$  of global aggregation  $g$  can be obtained as

$$T_{m;[g,k]}^{\langle j \rangle} = \max_{n \in \mathcal{N}_{m;[g]}^{\langle j \rangle}} \left\{ t_{m,n;[g,k]}^{\text{end},\langle j \rangle} \right\}. \quad (13)$$

### B. Modeling the Time Overhead of Global Iterations

When an ES completes the edge training of task  $j$ , the edge model will be transmitted to CS for global aggregation. We denote the upload time from ES  $m$  to the CS as

$$t_m^{E2C,\langle j \rangle} = I_m^{E2C,\langle j \rangle} / r_m^{E2C}, \quad (14)$$

where  $I_m^{E2C,\langle j \rangle}$  represents the size of edge model, and  $r_m^{E2C}$  represents the data rate of ES  $m$  to CS, which is assumed to be time-invariant as these communications often take place over the backhaul network wired links. Then, we can get the time required for each task to complete one round of global iteration at ES  $m$ , as given by

$$T_{m;[g]}^{\langle j \rangle} = t_m^{E2C,\langle j \rangle} + \sum_{k=1}^{K^{\langle j \rangle}} T_{m;[g,k]}^{\langle j \rangle}. \quad (15)$$

## IV. PROBLEM FORMULATION AND DESIGN OF HEART

In this section, we first provide the key constraints that are involved in our scenario of interest. Then, we present our problem formulation and explain our solution method.

### A. Key Constraint Design

In the IoV context, one key concern is ensuring that vehicles complete their training tasks and transmit the results to the corresponding ES promptly, mitigating potential negative impacts on training performance caused by network dynamics. Accordingly, we introduce a constraint given by

$$\sum_{j \in \mathcal{J}} \sum_{k \in K^{\langle j \rangle}} t_{m,n;[g,k]}^{\langle j \rangle} \bar{x}_{m,n;[g]}^{\langle j \rangle} < t_{m,n;[g]}^{\text{stay}}, \quad (16)$$

where  $t_{m,n;[g]}^{\text{stay}}$  represents the dwell time of the  $n^{\text{th}}$  vehicle within its associated ES  $m$  coverage, where  $\bar{x}_{m,n;[g]}^{\langle j \rangle} \in \{0, 1\}$  is defined in Sec. III-A. Next, we focus on imposing balance

across the training of different tasks. To reach this, we let  $\sum_{m \in \mathcal{M}_g^{\langle j \rangle}} \sum_{n \in \mathcal{N}_{m;[g,k]}^{\langle j \rangle}} \bar{x}_{m,n;[g]}^{\langle j \rangle}$  denote the number of times that task  $j$  has been assigned/trained at the  $g^{\text{th}}$  global iteration. Subsequently, we impose the training balance across the tasks via the following constraint

$$\frac{N}{J} - \xi_1 \leq \sum_{m \in \mathcal{M}_g^{\langle j \rangle}} \sum_{n \in \mathcal{N}_{m;[g,k]}^{\langle j \rangle}} \bar{x}_{m,n;[g]}^{\langle j \rangle} \leq \frac{N}{J} + \xi_2, \quad \forall j \in \mathcal{J}. \quad (17)$$

In (17),  $\xi_1, \xi_2 \in \mathbb{N}^+$  are adjustment coefficients. This constraint is inspired by the fact that achieving the pure fairness across the tasks, which equivalents to distributing all tasks evenly to vehicles (e.g., during a global iteration, each task will be trained by  $\frac{N}{J}$  vehicles) is not practical due to variations in the time vehicles remain within the edge coverage and the training time required for each task across different vehicles, which in turn depends on the task complexity. To address this, we constrain the number of times each task is assigned for training within a range centered around the average value  $\frac{N}{J}$ . Specifically, the left side of the equation denotes the lower bound on the number of times task  $j$  is assigned for training, while the right side represents the upper bound. This approach aims to achieve task scheduling fairness considering the dynamic nature of vehicle availability.

### B. Optimization Problem of Our Interest

We next focus on optimizing the latency of the entire process taken place in each round of global iteration (e.g., the  $g^{\text{th}}$  round). Our major goal is to obtain task scheduling at each vehicle  $\bar{x}_{m,n;[g]}^{\langle j \rangle}$  and training sequence  $\lambda_{m,n;[g,k]}$ , upon considering mobility of vehicles and task training balance, which we formulate through the following optimization problem

$$\mathcal{P} : \underset{\bar{x}_{m,n;[g]}^{\langle j \rangle}, \lambda_{m,n;[g,k]}}{\text{argmin}} \left\{ \max_{j \in \mathcal{J}, m \in \mathcal{M}_g^{\langle j \rangle}} \{T_{m;[g]}^{\langle j \rangle}\} \right\} \quad (18)$$

s.t. (16), (17)

Integrating asynchronous aggregation rule in the CS, in this formulation, we aim to optimize  $\bar{x}_{m,n;[g]}^{\langle j \rangle}$  and  $\lambda_{m,n;[g,k]}$  for all the vehicles  $n$ , ESs  $m$ , and tasks  $j$  so as to minimize the cumulative time required for all the tasks to undergo a complete round of global iteration, which is captured by the objective function, thereby reducing the time cost of the entire VEC-HFL process.

### C. Proposed Stagewise Scheduling through Hybrid Evolutionary And gReedy allocation (HEART)

Due to the integer/discrete nature of the optimization variables,  $\mathcal{P}$  belongs to a sub-category of integer programming problems which are known to be NP-hard. To tackle this problem, we propose a stagewise scheduling method called HEART, designed to achieve a near-optimal solution in a timely manner.

In HEART, problem  $\mathcal{P}$  is solved in two stages. In *Stage 1*, we primarily address the task scheduling problem, which includes scheduling tasks to appropriate vehicles and ensuring balanced task training across the system. For this stage, we propose a hybrid heuristic approach that combines an improved

Particle Swarm Optimization (PSO) algorithm with a Genetic Algorithm (GA). By integrating crossover and mutation operations from GA into PSO, our method enhances global search capabilities and explores a broader solution space, significantly reducing the risk of getting trapped in local optima. In *Stage 2*, we focus on optimizing the training sequence/rank of the assigned tasks on each vehicle, ensuring that the tasks are trained in an appropriate order to minimize delays. Besides, to guarantee that the vehicles' task training sequence accounts for both task overlap and model upload time, we introduce the concept of a task training scheduling combination score. We will aim to maximize this score at the edge by optimizing the vehicles' task training sequence through an efficient greedy algorithm.

### Stage 1: Task Scheduling via a Hybrid Heuristic Approach

Heuristic algorithms such as PSO and GA are widely used due to their exceptional performance in scheduling and resource allocation problems [18], [19]. However, the complexity inherent in these problems, particularly the one considered in Stage 1 of this paper, often causes these algorithms to get trapped in local optima when they are used in isolation. To overcome this challenge, we propose a hybrid optimization algorithm that leverages the complementary strengths of both PSO and GA. In conventional PSO, particles tend to cluster prematurely, which weakens the algorithm's global search capability [20], [21]. Meanwhile, GA requires careful parameter tuning and frequently suffers from premature convergence [22], [23]. By integrating these two methods, we strive to achieve solutions that are globally optimal—or at least near-optimal—and avoid the pitfalls commonly associated with using a single method.

Our proposed hybrid PSO-GA introduces two key enhancements. First, we replace the static inertia weight in PSO with a dynamic adjustment mechanism, enabling the swarm to adapt more effectively to complex, evolving search spaces. Second, we refine the GA's mutation process and strengthen its constraints. These refinements boost our hybrid algorithm's ability to explore a broader range of potential solutions, thereby reducing the likelihood of converging to suboptimal solutions.

In the following, we first provide an overview and sketch of the modifications we made to the PSO framework in S1.1. Then, we provide an overview and sketch of the modifications we made to the GA framework in S1.2. Next, we provide a detailed description of our hybrid PSO-GA approach integrating these modifications in S1.3. We later demonstrate through numerical simulations that our hybrid PSO-GA can more effectively discover high-quality solutions compared to standard heuristic methods.

*S1.1 Overview and sketch of the PSO process:* In our proposed task scheduling framework, a conventional PSO algorithm would search for optimal scheduling solutions across all vehicles at once [18], [20]. In particular, conventional PSO, inspired by the social behavior of bird flocks or fish schools, operates by having particles (representing solutions) move through the solution space. Each particle adjusts its position based on its own experience and that of its neighbors, guided by a *fitness function* that evaluates solution quality. The algorithm iteratively refines particle positions to converge on an optimal or near-optimal solution. While this global

approach captures overall system objectives, it significantly increases the algorithm's complexity and makes it difficult to tailor the scheduling solution for each individual vehicle in our setting of interest. Conversely, assigning tasks on a per-vehicle basis risks neglecting the overarching need for balanced global task allocation. A particular challenge arises because assigning more tasks can provide richer training data—beneficial for building a high performance global model—but since different tasks require different training times, within a limited dwell time, vehicles may often end up choosing tasks with shorter training durations to fit in as many tasks as possible when task assignments are made on a per-vehicle basis. As a result, tasks that take longer to train will be assigned less frequently, slowing down the progression of the global model accuracy and increasing the total training time. In the following, we detail our proposed enhanced PSO.

- *Design of an enhanced fitness function.* To address the issues discussed above, we redesign the fitness function in PSO to better balance local (per-vehicle) and global task distributions (a natural outcome will be to satisfy the task scheduling constraint (17), while reaching a near-optimal value for the objective function in (18)). In our method, we continuously optimize each vehicle's fitness function to find an appropriate task scheduling solution. We also incorporate a *task weight coefficient*  $\rho_j$ , which increases the reward for assigning tasks with longer training durations. This mechanism ensures that shorter-duration tasks do not overshadow more time-intensive tasks. By doing so, we achieve an equitable distribution of tasks across vehicles and maintain a high overall system performance. Through the above two strategies, our algorithm more effectively balances scheduling decisions, thus improving both training efficiency and convergence toward the global model accuracy. In particular, we formalize the fitness function of vehicle  $n$  under the coverage of edge server  $m$  in the  $g^{\text{th}}$  global iteration as follows:

$$f_{m,n;[g]} = \begin{cases} -\infty & \text{if it can not meet (16)} \\ \sum_{j=1}^J \bar{x}_{m,n;[g]}^{(j)} - (\xi_3 \sum_{j=1}^J |\psi_j - \chi| - \sum_{j=1}^J \rho_j |\psi_j - \chi|) & \text{otherwise} \end{cases}. \quad (19)$$

In (19),  $\sum_{j=1}^J |\psi_j - \chi|$  serves as a penalty for imbalanced task assignments. Here,  $\psi_j$  is a binary variable that indicates whether task  $j$  has been assigned (e.g., when  $\bar{x}_{m,n;[g]}^{(j)} = 1$ ,  $\psi_j = 1$ ,  $j \in J$ ), and  $\chi$  represents the target number of assignments for each task. Thus,  $|\psi_j - \chi|$  measures the discrepancy between the actual assignment and the ideal allocation. Additionally,  $\xi_3$  is a balance factor that influences the importance of minimizing this discrepancy. For each vehicle, we define the task scheduling corresponding to the global optimal fitness value  $f_{m,n;[g]}^{\text{global}}$  as the vehicle's task scheduling (i.e.,  $\bar{x}_{m,n;[g]}^{\text{global},(j)}$ ). In addition, this value will be used to update the particle's task scheduling along with the local optimal fitness value  $f_{m,n;[g]}^{p,\text{local}}$  of each particle. These variables are randomly initialized at the beginning of the PSO process.

- *Enhancing the inertia weight.* Traditional PSO uses a constant inertia weight  $\pi$  to moderate the velocity of the particles, preventing them from moving too quickly or too slowly. Although this constant weight helps with extreme search bias, it

also suffers from several drawbacks: it cannot adapt to dynamic changes in the environment, it is more prone to premature convergence, and it limits the algorithm's exploratory ability. To address these issues, we introduce a linear descent mechanism for updating the inertia weight. By gradually decreasing  $\pi$  over the course of the iterations, the swarm initially benefits from a larger momentum that aids in exploring a wide region of the solution space. As the search progresses, the decreasing inertia weight allows the particles to fine-tune their convergence, thus reducing the risk of stagnating in suboptimal solutions. Mathematically, we modify the inertia weight as follows:

$$\pi(\tau) = \pi_{\max} - \frac{\pi_{\max} - \pi_{\min}}{\tau^*} \tau, \quad (20)$$

where,  $\pi_{\max}$  and  $\pi_{\min}$  define the upper and lower bounds of the inertia weight, respectively, while  $\tau^*$  is the total number of iterations and  $\tau$  represents the current iteration index. Using (20), in the initial phase of the optimization process, the inertia weight starts at a high value to promote broad exploration of the search space. As the algorithm advances, the inertia weight gradually decreases, shifting the focus toward more refined local convergence. This adaptive behavior increases the overall efficiency of the algorithm at different stages and aids in identifying an optimal task scheduling plan.

• *Update of velocity and task scheduling.* Next, we update the velocity  $v$  in the  $\tau^{\text{th}}$  PSO process through  $\pi(\tau)$  and the task scheduling  $\bar{x}_{m,n;[g]}^{p,\langle j \rangle}(\tau - 1)$  for each particle in the previous iteration, and update the position of the particles accordingly (i.e., the task scheduling  $\bar{x}_{m,n;[g]}^{p,\langle j \rangle}(\tau - 1)$ ). Firstly, the velocity for particle  $p$  in the  $\tau^{\text{th}}$  iteration is given by

$$v_{m,n;[g]}^{p,\langle j \rangle}(\tau) = \pi(\tau - 1)v_{m,n;[g]}^{p,\langle j \rangle}(\tau - 1) + \xi_4\{\bar{x}_{m,n;[g]}^{p,\text{local},\langle j \rangle} - \bar{x}_{m,n;[g]}^{p,\langle j \rangle}(\tau - 1)\} + \xi_5\{\bar{x}_{m,n;[g]}^{\text{global},\langle j \rangle} - \bar{x}_{m,n;[g]}^{p,\langle j \rangle}(\tau - 1)\}, \quad (21)$$

where  $\xi_4, \xi_5 \in [0, 2]$  capture the social cognitive impact during PSO process, while  $\bar{x}_{m,n;[g]}^{p,\text{local},\langle j \rangle}$  represents the local optimal task scheduling for each particle, and  $\bar{x}_{m,n;[g]}^{\text{global},\langle j \rangle}$  is the global optimal task scheduling of the vehicle. Before the PSO process begins, we will randomly initialize these and update them later. Then, we introduce  $\Phi_{m,n;[g]}^{p,\langle j \rangle}(\tau)$  to represent the probability of the current task being assigned and use it to update the task scheduling of particle  $p$  as follows:

$$\Phi_{m,n;[g]}^{p,\langle j \rangle}(\tau) = \frac{1}{1 + e^{-v_{m,n;[g]}^{p,\langle j \rangle}(\tau)}}, \quad (22)$$

$$\bar{x}_{m,n;[g]}^{p,\langle j \rangle}(\tau) = \begin{cases} 1 & \text{if } e_1 \leq \Phi_{m,n;[g]}^{p,\langle j \rangle}(\tau) \\ 0 & \text{otherwise} \end{cases}, \quad (23)$$

where  $e_1$  is a random value in the range  $[0, 1]$ . We obtain  $\bar{x}_{m,n;[g]}^{p,\langle j \rangle}(\tau)$  through (23) and use it in (19) to calculate the fitness value  $f_{m,n;[g]}^p(\tau)$  of the particle, and decide whether to update  $\bar{x}_{m,n;[g]}^{p,\text{local},\langle j \rangle}$ ,  $\bar{x}_{m,n;[g]}^{\text{global},\langle j \rangle}$ ,  $f_{m,n;[g]}^{p,\text{local}}$ ,  $f_{m,n;[g]}^{\text{global}}$  (later concerntized in the algorithm description).

Despite the advancements we made to PSO, it may still encounter challenges in global exploration. To address this, we integrate a GA step – as discussed below – between particle updates, thereby enhancing global search capabilities.

At the same time, the PSO framework bolsters the GA by continuously refining the search for the global optimum. This hybrid approach effectively balances exploration and exploitation, leading to improved task scheduling solutions in complex optimization scenarios of our interest in this work.

• *1.2 Overview and sketch of the GA process:* Traditional GA generally includes steps such as fitness evaluation, selection, crossover, mutation, and other operations. However, because the PSO component in our hybrid system already handles fitness evaluation, we streamline the GA portion to just two steps at the end of each PSO cycle: (i) Crossover and (ii) Mutation. These operations help diversify the swarm by introducing new task scheduling patterns and reducing the risk of converging prematurely to local optima.

• *Crossover enhancement.* During the task scheduling phase for each vehicle, we sequentially select two adjacent particles,  $p$  and  $p + 1$ , correspond to task scheduling  $\bar{x}_{m,n;[g]}^{p,\langle j \rangle}(\tau)$ ,  $\bar{x}_{m,n;[g]}^{p+1,\langle j \rangle}(\tau)$ . We then apply crossover and mutation on these allocations repeatedly. Specifically, for crossover,  $p$  and  $p + 1$  serve as parent solutions, and we define a genetic length  $J$  along with a randomly chosen crossover point  $r$  such that  $1 < r < J$ . Exchanging the segments of the parent allocations at the crossover point creates two offspring,  $c_1$  and  $c_2$ . Thus, new task scheduling schemes are generated, which expand the exploration space and reduce the likelihood of trapping the algorithm in suboptimal solutions. We define all task scheduling for  $p, p + 1$  as a vector  $X_{m,n;[g]}^p(\tau)$  and  $X_{m,n;[g]}^{p+1}(\tau)$  (e.g., for  $p$  during the  $\tau^{\text{th}}$  iteration, if the particle implies the scheduling of tasks 1, 3, and 4 out of the four available tasks in the system, we will have the vector  $X_{m,n;[g]}^p(\tau) = [1, 0, 1, 1]$ ). To better describe this crossover process, we use  $[i : j]$  to represent the elements from  $i$  to  $j - 1$  in the vector, e.g., considering  $X_{m,n;[g]}^p(\tau) = [1, 0, 1, 1]$ , we have  $X_{m,n;[g]}^p(\tau)[0 : 2] = 1, 0$ . We then obtain the offspring inherit allocations from the parents according to the following crossover rules:

$$X_{m,n;[g]}^{p,c_1}(\tau) = [X_{m,n;[g]}^p(\tau)[0 : r], X_{m,n;[g]}^{p+1}(\tau)[r : J]], \quad (24)$$

$$X_{m,n;[g]}^{p+1,c_2}(\tau) = [X_{m,n;[g]}^{p+1}(\tau)[0 : r], X_{m,n;[g]}^p(\tau)[r : J]], \quad (25)$$

where  $X_{m,n;[g]}^{p,c_1}(\tau), X_{m,n;[g]}^{p+1,c_2}(\tau)$  represents the vector of task scheduling for the offsprings, and the single task scheduling  $\bar{x}_{m,n;[g]}^{p,\langle j \rangle,c_1}(\tau)$  and  $\bar{x}_{m,n;[g]}^{p+1,\langle j \rangle,c_2}(\tau)$  are the  $j^{\text{th}}$  elements of these vectors.

• *Mutation enhancement.* For the newly generated offspring  $c_1$  and  $c_2$  in (24) and (25), we further expand the solution space for each particle by applying mutation operations: whether these offsprings also undergo mutation is determined by a mutation rate  $\varphi$ . Nevertheless, a constant  $\varphi$  is less flexible and cannot accommodate different exploration needs across various search stages. Therefore, we define an adaptive mutation rate based on the number of iterations  $\tau$ , i.e.,  $\varphi(\tau) = \frac{\varphi_{\max}}{1 + \log(1 + \tau)}$ . During the initial phase, a higher mutation rate promotes broad global exploration, reducing the risk of convergence to local optima. As the number of iterations increases,  $\varphi(\tau)$  decreases, aiding the algorithm in fine-tuning its convergence process. To introduce additional randomness and broaden the global search, we compare a random factor against  $\varphi(\tau)$  to determine if a

mutation occurs. For example, for offspring  $c_1$ , the mutation decision is governed by the following rule:

$$\bar{x}_{m,n;[g]}^{p,\langle j \rangle}(\tau) \leftarrow \begin{cases} 1 - \bar{x}_{m,n;[g]}^{p,\langle j \rangle, c_1}(\tau) & \text{if } e_2 < \varphi(\tau) \\ \bar{x}_{m,n;[g]}^{p,\langle j \rangle}(\tau) & \text{otherwise} \end{cases}, \quad (26)$$

where  $e_2$  is a random value in the range [0,1]. Although the GA stage can generate novel task scheduling schemes, these new allocations may cause the total time required to complete all assigned tasks to exceed the vehicle's available time under ES  $m$ 's coverage, as constrained by (16), which we will take into account in our overarching method described next.

---

**Algorithm 2:** Design of hybrid heuristic by integrating improved PSO and GA in Stage 1

---

```

Input :  $t_{m,n;[g,k],h}^{(j)}$ ,  $t_{m,n;[g]}^{stay}$ ,  $p^*$ ,  $\tau^*$ ,  $\rho_j$ ,  $\chi$ ,  $\pi_{max}$ ,  $\pi_{min}$ ;
Output:  $\bar{x}_{m,n;[g]}^{global,\langle j \rangle}$ ;
Initialization :  $\bar{x}_{m,n;[g]}^{p,\langle j \rangle}(0)$ ,  $v_{m,n;[g]}^{p,\langle j \rangle}(0)$ ,  $\bar{x}_{m,n;[g]}^{p,local,\langle j \rangle}$ ,
 $\bar{x}_{m,n;[g]}^{global,\langle j \rangle}$ ,  $f_{m,n;[g]}^{p,local}$ ,  $f_{m,n;[g]}^{global}$ ;
foreach  $n \in \mathcal{N}$  do
  for  $\tau = \{1, 2, \dots, \tau^*\}$  do
    PSO process:
      Dynamically adjust  $\pi(\tau)$  based on (20)
      for  $p = \{1, 2, \dots, p^*\}$  do
        Obtain the task scheduling  $\bar{x}_{m,n;[g]}^{p,\langle j \rangle}(\tau)$  for the
        current particle based on (21)-(23)
        Based on  $\bar{x}_{m,n;[g]}^{p,\langle j \rangle}(\tau)$  and (19) calculate the
        fitness  $f_{m,n;[g]}^p(\tau)$ 
        if  $f_{m,n;[g]}^p(\tau) > f_{m,n;[g]}^{p,local}$  then
           $\bar{x}_{m,n;[g]}^{p,local,\langle j \rangle} \leftarrow \bar{x}_{m,n;[g]}^{p,\langle j \rangle}(\tau)$ ,
           $f_{m,n;[g]}^{p,local} \leftarrow f_{m,n;[g]}^p(\tau)$ 
          if  $f_{m,n;[g]}^p(\tau) > f_{m,n;[g]}^{global}$  then
             $\bar{x}_{m,n;[g]}^{global,\langle j \rangle} \leftarrow \bar{x}_{m,n;[g]}^{p,\langle j \rangle}(\tau)$ ,  $f_{m,n;[g]}^{global} \leftarrow$ 
             $f_{m,n;[g]}^p(\tau)$ 
        GA process:
        for  $p = 1$  to  $(p^* - 1)$  do
          Crossover enhancement: based on (24) and (25)
          get  $\bar{x}_{m,n;[g]}^{p,\langle j \rangle, c_1}(\tau)$ ,  $\bar{x}_{m,n;[g]}^{p+1,\langle j \rangle, c_2}(\tau)$ 
          Mutation enhancement: based on (26) get
           $\bar{x}_{m,n;[g]}^{p,\langle j \rangle}(\tau)$ ,  $\bar{x}_{m,n;[g]}^{p+1,\langle j \rangle}(\tau)$ 
          if task scheduling  $\bar{x}_{m,n;[g]}^{p,\langle j \rangle}(\tau)$ ,  $\bar{x}_{m,n;[g]}^{p+1,\langle j \rangle}(\tau)$ 
          do not meet constraint (16) then
            Exclude the task with the longest training
            time from  $\bar{x}_{m,n;[g]}^{p,\langle j \rangle}(\tau)$ ,  $\bar{x}_{m,n;[g]}^{p+1,\langle j \rangle}(\tau)$ 
            until the constraint is met

```

---

*S1.3 Detail of our proposed hybrid heuristic approach:* Our proposed method combines the above PSO and GA processes. Below, we provide the description of our method, where its steps are summarized in Alg. 2:

**Step 1. Initialization:** Our method starts with randomly initializing (i) the task scheduling  $\bar{x}_{m,n;[g]}^{p,\langle j \rangle}(0)$  for each particle  $p$  while satisfying constraint (16) and the velocity  $v_{m,n;[g]}^{p,\langle j \rangle}(0)$ , (ii) the local optimal task scheduling  $\bar{x}_{m,n;[g]}^{p,local,\langle j \rangle}$  (iii) the local

optimal fitness  $f_{m,n;[g]}^{p,local}$  of each particle  $p$ , (iv) the global optimal task scheduling  $\bar{x}_{m,n;[g]}^{global,\langle j \rangle}$  (i.e., the task scheduling of the vehicle), and (v) the global optimal fitness  $f_{m,n;[g]}^{global}$  of all particles.

**Step 2. Implementing PSO Process:** In each iteration, the adaptive inertia weight  $\pi(\tau)$  is obtained according to (20). For each particle  $p$ , the velocity  $v_{m,n;[g]}^{p,\langle j \rangle}(\tau)$  is first calculated based on (21). Then, the probability of each task being assigned  $\Phi_{m,n;[g]}^{p,\langle j \rangle}(\tau)$  is calculated using (22), and the task scheduling  $\bar{x}_{m,n;[g]}^{p,\langle j \rangle}(\tau)$  is obtained via (23) (lines 7-8, Alg. 2). Next, the fitness value  $f_{m,n;[g]}^p(\tau)$  of the particle is computed based on (19) and compared with  $f_{m,n;[g]}^{p,local}$  of the particle and  $f_{m,n;[g]}^{global}$  of all particles, according to which the following conditions may occur (lines 10-12, Alg. 2):

**Condition 1.** If  $f_{m,n;[g]}^p(\tau)$  is greater than  $f_{m,n;[g]}^{p,local}$  and  $f_{m,n;[g]}^{global}$ , it implies the high quality of the task scheduling associated with particle  $p$ . Subsequently, we perform the following updates:  $\bar{x}_{m,n;[g]}^{local,\langle j \rangle} \leftarrow \bar{x}_{m,n;[g]}^{p,\langle j \rangle}(\tau)$  and  $f_{m,n;[g]}^{p,local} \leftarrow f_{m,n;[g]}^p(\tau)$ ;  $\bar{x}_{m,n;[g]}^{global,\langle j \rangle} \leftarrow \bar{x}_{m,n;[g]}^{p,\langle j \rangle}(\tau)$  and  $f_{m,n;[g]}^{global} \leftarrow f_{m,n;[g]}^p(\tau)$ .

**Condition 2.** If  $f_{m,n;[g]}^p(\tau)$  is greater than  $f_{m,n;[g]}^{p,local}$  but lower than  $f_{m,n;[g]}^{global}$ , it implies the local optimality of the particle. Subsequently, we perform  $\bar{x}_{m,n;[g]}^{local,\langle j \rangle} \leftarrow \bar{x}_{m,n;[g]}^{p,\langle j \rangle}(\tau)$ .

**Condition 3.** If  $f_{m,n;[g]}^p(\tau)$  is lower than  $f_{m,n;[g]}^{p,local}$  and  $f_{m,n;[g]}^{global}$ , it implies the low quality of the particle. Subsequently, no update will be triggered.

**Step 3. Implementing GA Process:** GA aims to increase the exploration space of the solution via conducting crossing and mutation on the task scheduling variable  $\bar{x}_{m,n;[g]}^{p,\langle j \rangle}(\tau)$  obtained from the PSO process. It selects two particles  $p$  and  $p + 1$  in sequence for these operations until all particles are covered (line 15, Alg. 2) to obtain the task scheduling vectors  $X_{m,n;[g]}^p(\tau)$  and  $X_{m,n;[g]}^{p+1}(\tau)$  for particles  $p$  and  $p + 1$  during the crossover process using the crossover point  $r$  for element swapping in the vectors (based on (24) and (25)). It then obtains the updated task scheduling variables  $\bar{x}_{m,n;[g]}^{p,\langle j \rangle, c_1}(\tau)$  and  $\bar{x}_{m,n;[g]}^{p+1,\langle j \rangle, c_2}(\tau)$ . It then executes the mutation operation which mainly flips the task scheduling decisions when randomly selected  $e_2$  is less than the adaptive mutation rate  $\varphi(\tau)$  (based on (26)). Through this operation, it obtains new task scheduling solutions  $\bar{x}_{m,n;[g]}^{p,\langle j \rangle}(\tau)$  and  $\bar{x}_{m,n;[g]}^{p+1,\langle j \rangle}(\tau)$ . In addition, if the new task scheduling solutions do not meet constraint (16), the task with the longest training time is removed until the constraint is met.

**Step 4. Repeat:** The above steps (i.e., Steps 1 to 3) are repeated for each vehicle to obtain the global optimal solution.

*Stage 2: Optimizing Task Training Rank via a Greedy Algorithm*

In our synchronous aggregation process at the ES, each vehicle uploads its locally trained model for task  $j$  upon completion, and the ES waits until it has received all models before performing edge aggregation. However, if the training rank of a vehicle for task  $j$  is improper, the ES would have to delay the update of the corresponding edge model, which prolongs

the overall training time and risks model obsolescence. Consequently, determining an optimal rank for tasks assigned to vehicles in the ES coverage area is critical for maximizing the time overlap among the vehicles processing the same task and thus minimizing the objective in (18). Nevertheless, when multiple task sequence combinations yield similarly high overlaps, the decision process becomes complex. Additionally, vehicle mobility and heterogeneous task model sizes further complicate this scheduling problem, as transmission times during edge iterations can vary depending on how quickly each training task is finished. Taken together, these factors highlight the need for an efficient, low-complexity approach to optimizing task training sequences/ranks, ensuring that training overlap is maximized while minimizing edge aggregation delays.

**S2.1 Determining the task training sequences/ranks:** To effectively determine the rank in which vehicles train their assigned tasks, we introduce the concept of *aggregate-score*. The optimal task training sequence/rank for each vehicle is perceived to be the one that achieves the highest aggregate-score, taking into account both task overlap and model upload time. This approach avoids ambiguities arising from multiple valid solutions and considers factors that affect the quality of the overall scheduling. In terms of *task overlap*, once the set of tasks that vehicle  $n$  must train under ES  $m$  in the  $g^{\text{th}}$  global iteration is determined in the above-described Stage 1 of our method, we first randomly initialize its training rank  $\lambda_{m,n;[g,k]}$ . To compute the overlap across the tasks, we define an *overlap indicator function*  $\delta(\lambda_{m,n;[g,k]}^{(j)}, \lambda_{m,n';[g,k]}^{(j)})$  for each task  $j$ . This function equals 1 if task  $j$  for vehicles  $n$  and  $n'$  that are both covered by ES  $m$  has the same rank (i.e.,  $\lambda_{m,n;[g,k]}^{(j)} = \lambda_{m,n';[g,k]}^{(j)}$ ), and 0 otherwise. For example, consider a scenario in which there are four tasks and two vehicles,  $n$  and  $n'$ . Vehicle  $n$  is assigned tasks by following the sequence/rank  $[1, 3, 4]$ , while vehicle  $n'$  is assigned tasks with  $[2, 3]$ . In this situation, only the second task indices overlap (both vehicles train task 3 in their second slots), making  $\delta(\lambda_{m,n;[g,k]}^{(3)}, \lambda_{m,n';[g,k]}^{(3)}) = 1$ , while the indicators of all other tasks are 0. During the  $k^{\text{th}}$  edge iteration, the overlap score for task  $j$ , denoted as  $\mathcal{S}_{m;[g,k]}^{\text{lap},(j)}$ , is then computed as the sum of the above indicator functions over all vehicles within each ES  $m$ 's coverage:

$$\mathcal{S}_{m;[g,k]}^{\text{lap},(j)} = \sum_{n, n' \in \mathcal{N}_{m;[g]}^{\text{cov}}, n \neq n'} \delta(\lambda_{m,n;[g,k]}^{(j)}, \lambda_{m,n';[g,k]}^{(j)}). \quad (27)$$

In principle, achieving the maximum overlap during task scheduling is desired: a higher task overlap allows vehicles to train the same task at close intervals, ensuring that the local model of the task at the corresponding ES can be aggregated and distributed in a timely manner, thereby reducing the occurrence of *case (ii)* described in Section III-A on the vehicle side, and thus reducing the durations of inactive periods. However, when multiple task training sequences coincide with the highest overlap, choosing the best sequence becomes non-trivial. Additionally, as discussed earlier, in *case (ii)*, the model upload time inevitably occurs, which further needs to be considered when deciding on task training sequence/rank. For example, when the vehicle within an ES's coverage is to move

away from the ES, it may be optimal to process the task that has the largest model size first – since the model transmission for this task can take place while the vehicle is still close to the ES and has a high data rate – while assigning the tasks that have smaller model sizes higher ranks (i.e., process them later). To consider this phenomenon, we first obtain the model upload time based on factors like the distance between the vehicle and edge server (ES)  $m$  and the size of the task model. Specially, when specifying a training sequence for a task, we first calculate the time cost  $t_{m,n;[g,k]}^{V2E,(j)}$  based on (8), and obtain the *model upload score*  $\mathcal{S}_{m,n;[g,k]}^{\text{up},(j)}$  as a function of the model upload time as follows:

$$\mathcal{S}_{m,n;[g,k]}^{\text{up},(j)} = \xi_6 / t_{m,n;[g,k]}^{V2E,(j)}, \quad (28)$$

where  $\xi_6$  is a positive coefficient, which adjusts the model upload score in (28) to the same level as the overlap score given by (27). This score is then combined with the task overlap score for each task  $j$  to get its aggregate-score, which is given by

$$\mathcal{S}_{m;[g,k]}^{\text{all},(j)} = \xi_7 \mathcal{S}_{m;[g,k]}^{\text{lap},(j)} + (1 - \xi_7) \sum_{n \in \mathcal{N}_{m;[g]}^{(j)}} \mathcal{S}_{m,n;[g,k]}^{\text{up},(j)}, \quad (29)$$

where  $\xi_7$  is a balance factor that weighs task overlap against model upload time. Finding the maximum aggregate-score for each task yields the order in which vehicles should train their tasks. However, determining a scheduling for all tasks under ES  $m$  coverage simultaneously is non-trivial due to its combinatorial nature. For example, if it is integrated into Stage 1 of our method, the complexity of PSO and the GA will increase rapidly. To this end, we propose a low-complexity greedy algorithm that sequentially ranks the tasks based on their aggregate-score, which can be executed in real-time.

**S2.2 Detail of the greedy-based task ranking solution:** For training sequence/rank optimization, it is necessary to maximize the aggregate-score  $\mathcal{S}_{m;[g,k]}^{\text{all},(j)}$  under each ES  $m$  coverage for each edge iteration  $k$ . Subsequently, maximization of aggregate-score can be decoupled and conducted in parallel across the ESs and edge iterations. As a result, we focus on a specific ES  $m$  and edge iteration  $k$  in the following.

Details of the entire process are provided below (also see Alg. 3):

**Step 1. Initialization:** The highest aggregate-score  $\mathcal{S}_{m;[g,k]}^*$  is initialized to zero, making the training sequence  $\lambda_{m,n;[g,k]}$  of each vehicle under ES  $m$  coverage an empty set, and the set  $\mathcal{J}'$  is initialized as  $\mathcal{J}' = \mathcal{J}$ . Also, variable  $q$  to represent the task with the highest  $\mathcal{S}_{m;[g,k]}^*$ , used in the following (line 1, Alg. 3).

**Step 2. Select proper task for  $\mathcal{S}_{m;[g,k]}^*$ :** For the unassigned task set  $\mathcal{J}'$  of ES  $m$ , our method checks through all the tasks and computes the overlap score  $\mathcal{S}_{m;[g,k]}^{\text{lap},(j)}$  based on (27) (line 5, Alg. 3) for each task  $j$ . It then goes over every vehicle under the coverage of ES that has this training task and obtains the upload time  $t_{m,n;[g,k]}^{V2E,(j)}$  based on (8). Afterwards, it calculates the model upload score  $\mathcal{S}_{m,n;[g,k]}^{\text{up},(j)}$  based on the  $t_{m,n;[g,k]}^{V2E,(j)}$  (using (28)) (lines 7 and 8, Alg. 3). Finally, it obtains  $\mathcal{S}_{m;[g,k]}^{\text{all},(j)}$  for this task (based on (29)) (line 9, Alg. 3). Next, it compares this value with  $\mathcal{S}_{m;[g,k]}^*$  (lines 10-12, Alg. 3), until task  $q$  with the

---

**Algorithm 3:** Greedy-based algorithm for training rank determination in Stage 2

---

```

Input :  $\bar{x}_{m,n;[g]}^{global,\langle j \rangle}$ ;
Output:  $\lambda_{m,n;[g,k]}$ ;
1 Initialization : Highest aggregate-score  $\mathcal{S}_{m;[g,k]}^* = 0$ ,  

 $\lambda_{m,n;[g,k]} = \emptyset$ ,  $q = 0$ ,  $\mathcal{J}' = \mathcal{J}$ ;
2 foreach  $m \in \mathcal{M}$  in parallel do
3   for  $k = \{1, 2, \dots, K^{\langle j \rangle}\}$ , where  $j \in \mathcal{J}$  do
4     for  $j \in \mathcal{J}'$  do
5       Calculate  $\mathcal{S}_{m;[g,k]}^{lap,\langle j \rangle}$  based on  $\bar{x}_{m,n;[g]}^{global,\langle j \rangle}$  and (27)
6       for  $n \in \mathcal{N}_{m;[g,k]}^{\langle j \rangle}$  do
7         Use (8) to obtain the model upload time  

 $t_{m,n;[g,k]}^{V2E,\langle j \rangle}$ 
8         Calculate  $\mathcal{S}_{m,n;[g,k]}^{up,\langle j \rangle}$  based on (28)
9         Calculate  $\mathcal{S}_{m;[g,k]}^{all,\langle j \rangle}$  based on (29)
10        if  $\mathcal{S}_{m;[g,k]}^{all,\langle j \rangle} > \mathcal{S}_{m;[g,k]}^*$  then
11           $\mathcal{S}_{m;[g,k]}^* \leftarrow \mathcal{S}_{m;[g,k]}^{all,\langle j \rangle}$ 
12           $q \leftarrow j$ 
13        for  $n \in \mathcal{N}_{m;[g,k]}^{\langle q \rangle}$  do
14          Add task  $q$  at the end of training sequence  

 $\lambda_{m,n;[g,k]}$ 
15         $\mathcal{J}' \leftarrow \mathcal{J}' \setminus \{q\}$ 
16         $\mathcal{S}_{m;[g,k]}^* = 0$ 

```

---

highest  $\mathcal{S}_{m;[g,k]}^*$  is selected. The vehicle that owns this task then adds it to the end of  $\lambda_{m,n;[g,k]}$  and  $\mathcal{S}_{m;[g,k]}^*$  is then reset to zero (lines 14-16, Alg. 3).

**Step 3. Repeat:** Task  $q$  is then removed from  $\mathcal{J}'$  and the above steps are repeated for the remaining tasks until all the tasks are placed in the training sequence of vehicles.

## V. NUMERICAL EVALUATIONS

The VEC-HFL architecture considered in our simulations contains 1 CS, 5 ESs, and 25 to 50 vehicles depending on the specific simulation setup, where the CS with the coverage of 5 km is the radius in located at the center of the area. We consider an area with 4 roads and 4 intersections where an ES with the coverage of 1 km is located at each intersection. Each vehicle moves at a constant speed in the road, and at each intersection it takes a turn at a direction chosen randomly. To capture diverse training tasks, we consider 4 different ML tasks: CIFAR-10 (trained on VGG16 neural network [24]), MNIST (trained on a convolutional neural network with 4 layers [5]), Driver Yawning (trained on ResNet-18 neural network [25]) and 20 Newsgroups (trained on LSTM neural network [26]). In particular, CIFAR-10 and MNIST are colored and grayscale image datasets for ten-category image classification, respectively [5], [27], Driver Yawning represents a dataset for yawning detection during driving [28], while 20 Newsgroups is a text dataset in natural language processing, with data spanning 20 distinct topics. The data rates of vehicle-to-edge and edge-to-vehicle communications are set according to the channel modeling in [17]. Other key parameters used in the simulations are listed in Table I.

To conduct performance evaluations, we consider three aspects of system performance: (i) balanced task training; (ii) model convergence for different tasks; and (iii) time efficiency. Further, to conduct comparative analysis, the following benchmark methods are considered (the time complexity of HEART:  $\mathcal{O}(N \times J \times p^* \times \tau^* + N \times J \times K^{\langle j \rangle})$ ):

- **Two-Stage Stochastic Optimization (TSSO):** This method randomly schedules training tasks under time constraints and assigns a random seed to each task, determining the training rank of the task. The time complexity of the method is  $\mathcal{O}(2N \times J \times \gamma)$ , where  $\gamma$  represents the max attempts.

- **Two-Stage Particle Swarm Optimization (TSPSO):** Task scheduling and training rank are determined by traditional PSO under time constraints and task training balance [18]. The time complexity of the method is  $\mathcal{O}(2N \times J \times p^* \times \tau^*)$ .

- **Two-Stage Genetic Algorithm (TSGA):** Task scheduling and training rank are determined by traditional GA under time constraints and task training balance [19]. The time complexity of the method is  $\mathcal{O}(2N \times J \times p^* \times \tau^*)$ .

- **Two-Stage Greedy Algorithm (TSGD):** On the premise of ensuring that the task training time does not exceed the vehicles' dwell times, the task scheduling score is calculated for each vehicle based on the task weight coefficient  $\rho_j$  and the number of times it is allocated. The task with a higher score is selected and assigned to the vehicle, and then the task is removed. The above operation continues until the task scheduling is completed. Afterwards, Alg. 3 is employed to further refine the solution. The time complexity of the method is  $\mathcal{O}(2N \times J \times K^{\langle j \rangle})$ ;  $K^{\langle j \rangle}$  is less than  $p^*$  and  $\tau^*$ .

TABLE I: Parameter settings [29], [30]

Parameter	Value	Parameter	Value
Number of training tasks $J$	4	Learning rate $\eta^{\langle j \rangle}$	0.001-0.005
Local iterations $H^{\langle j \rangle}$	4-6	Edge iterations $K^{\langle j \rangle}$	8-10
Number of CPU cycles $c_n^{\langle j \rangle}$	20-30	Clock frequency $f_{m,n}^{\langle j \rangle}$	[1,10] GHz
Number of particles $p^*$	30	Iteration times $\tau^*$	100
Crossover point $r$	2	Initial mutation rate $\varphi_{max}$	0.3

We first start with evaluating the balance of task execution. To this end, we calculate the average task execution per round of global iteration for two scenarios: one involving 4 tasks and the other involving 9 tasks<sup>2</sup>. In particular, the left subplot of Fig. 3 illustrates the average number of times that tasks have been assigned over vehicles for training upon having 4 tasks. It can be observed that both traditional TSPSO and TSGA tend to get trapped in local optima, leading to uneven task execution distribution. This imbalance results in some tasks being executed on more vehicles, while others being executed on fewer vehicles, which negatively affects the task processing balance. Focusing on TSGD and TSSO, TSGD sequentially

<sup>2</sup>For the setting of 4 tasks, each vehicle is allocated with all data labels from the dataset, and own an equal number of data samples assigned to each label. For the setting of 9 tasks, we randomly select a subset of labels from the dataset and assign varying numbers of samples to each vehicle, e.g., tasks 7 and 9 are both CIFAR on CNN, but they are only assigned 5-7 labels, where the data samples of each label is random.

searches for the highest task scheduling score for each task, without a global search mechanism. Therefore, it is easy to fall into a local solution or be unable to backtrack on the choices made. As a result, in the left subplot of the figure, we observe that its allocation for task 3 is still not ideal, and *TSSO* has the worst performance because it relies on random selection method without any optimization. Thanks to the well-designed constraint on balanced scheduling, our proposed *HEART* can achieve far better performance in distributing diverse tasks over moving vehicles. To further validate the balance of task allocation, we apply 9 different data sample sizes and label partitioning methods on the above 4 tasks (the training time of each task becomes unique), forming 9 tasks. We then compare the balance on task scheduling on these 9 tasks across different methods in the right subplot of Fig. 3, from which a similar conclusion to the left subplot can be drawn, where *HEART* outperforms all the benchmark methods in terms of the balance of task execution.

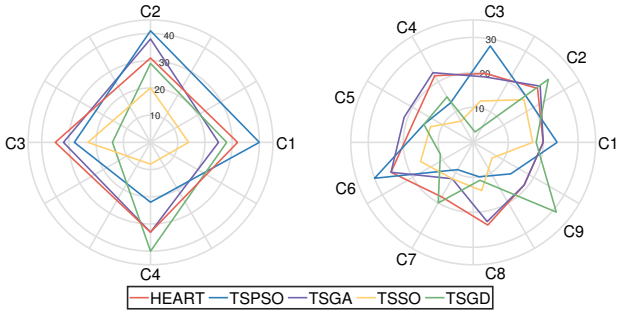


Fig. 3: The average number of times that a task has been executed on vehicles for training across different methods. Left subplot: 4 tasks where C1= CIFAR task; C2= MNIST task; C3= Driver Yawning task; C4= 20 Newsgroups task; Right subplot: 9 tasks that combine different amounts of data and labels for tasks C1-C4.

In Fig. 4, we study the model accuracy performance of various methods. We set the desired accuracy for the 4 tasks at 0.75, 0.9, 0.9, and 0.75, respectively, which are shown through the dotted horizontal lines in subfigures of Fig. 4. These desired accuracies are further used in the subsequent results. Besides, in the legends of the plots, we use *ComplT* to represent the wall-clock time at the instant of finishing of each task (e.g., task CIFAR in plot Fig. 4(a)). Also, we highlight the time in which the last task gets completed in each method via the red color in the legends (e.g., as in plot Fig. 4(b)), *TSSO* finishes the processing of all tasks through the execution of MNIST and the finish time is 215.8s). As shown in Fig. 4, our method completes the MNIST task training at 49.8s, the Driver Yawning task training at 74.7s, the CIFAR task training at 99.3s, and the time required to complete four task training is 110.2s, which is when the execution of 20 Newsgroup task completes. An interesting observation from Fig. 4 is that our method does not necessarily lead to the fastest convergence of all the tasks when the convergence speed is measured through the accuracy vs the global iteration. This is mainly due to the fact that our method balances the resource allocation across all the tasks, leading to a uniform convergence speed across all the tasks. Nevertheless, focusing on the values highlighted by red, our method leads to the fastest finish of execution of

all tasks when the convergence speed is measured though the wall-clock time (our method finishes all the task in 110.2s, which is notable lower than 191.9s for *TSPSO*, 154.1s for *TSGA*, 215.8s for *TSSO*, and 170.7s for *TSGD*). This unveils the power of balanced task execution in reducing the overall task completion through similar convergence speeds across different tasks. The rapid convergence of a specific task, as illustrated in Fig. 4(a) with examples like *TSPSO* and *TSGD*, is often due to prioritizing that task at the expense of others. In particular, assigning more vehicles to a particular task can indeed improve its convergence rate; however, this can lead to an imbalance across tasks, ultimately compromising equitable performance distribution. For example, in the left subplot of Fig. 3, we can see that the *TSGD* performs poorly on Driver Yawning, failing to achieve the expected accuracy (Fig. 4(c)). In a summary, our proposed *HEART* achieves the best convergence speed in terms of wall-clock time across all the baselines (Fig. 4) while keeping a balanced scheduling (Fig. 3).

The performance in terms of time efficiency captured via the overall time overhead (the time for all task models to reach the aforementioned desired accuracies) is shown in Fig. 5, upon testing various numbers of vehicles, where our method *HEART*, outperforms other methods. For example, we can achieve an average reduction of overall time overhead by 17.2%, 24.9%, 24.4% and 30.6% as compared to *TSGA*, *TSPSO*, *TSSO* and *TSGD* in Fig. 5(a) with 25 vehicles; and a reduction in overall time overhead by 18.3%, 24.7%, 34.59% and 36.76% in Fig. 5(b) when considering 50 vehicles. Interestingly, Fig. 5 shows that time cost is not always affected by the increase in data volume per vehicle. This is because the increase of data volume increases local training time, but also reduces the number of global iterations required to hit the target accuracy.

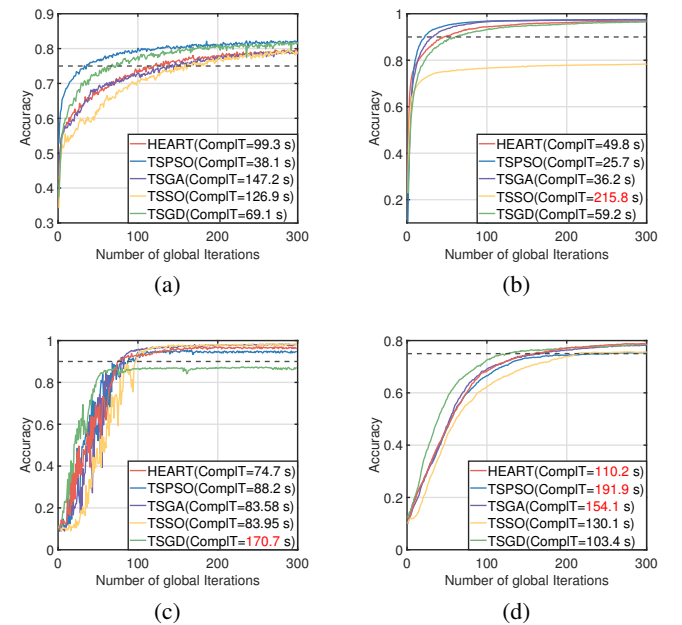


Fig. 4: Test accuracy of the global models for different tasks: (a) CIFAR; (b) MNIST; (c) Driver Yawning; (d) 20 Newsgroups.

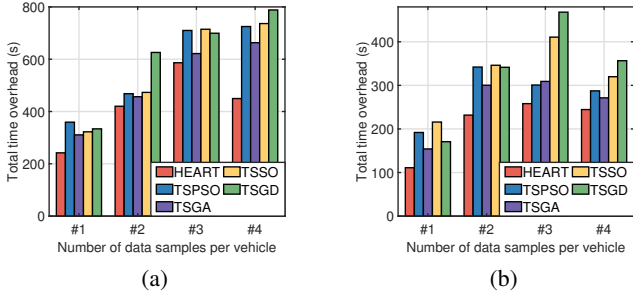


Fig. 5: The time that it takes for the global model of all tasks to achieve the fixed accuracy under different vehicle numbers, data samples per vehicles, and different methods: (a) 25 vehicles, and (b) 50 vehicles. Note that #1-#4 represent the number of 4 different data samples that the vehicle has for each task, which are 200, 400, 600, 800.

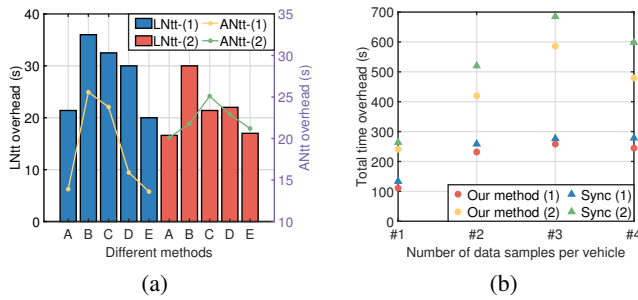


Fig. 6: Evaluations on non-task-training time overhead:(a) The average and the longest non-task-training time among all ESs; (b) The overall time overhead of hybrid aggregation rule and synchronous aggregation rule. Specifically, A, B, C, D and E represent HEART, TSGA, TPSO, TSSO, TSGD, (1) and (2) represent cases with 25 vehicles and 50 vehicles.

Fig. 6(a) illustrates the performance in terms of the non-task-training time (abbreviated as Ntt for simplicity) across different methods, including the average (abbreviated as ANtt) and the longest non-task-training time (abbreviated as LNtt) for all ESs per global iteration. Upon considering 25 vehicles, compared to TSGA, TPSO, and TSSO, the ANtt of HEART is lower by 51.7%, 41.5%, and 12.6%, and its LNtt is lower by 40.1%, 34.2%, and 28.6%. For 50 vehicles, our proposed HEART achieves 7.7%, 19.9%, and 12.2% reduction of ANtt; as well as 44.6%, 22.4%, and 24.5% reduction of LNtt when compared with the 4 baseline methods. We note that, since HEART and TSGD both employ the same optimization algorithm in Stage 2, their performance outcomes are relatively similar, however, as shown in Fig. 3 and 5 our method exhibits a better time efficiency and task execution balance. These results demonstrate that our approach effectively reduces overall non-task-training time and accelerates the completion of edge iterations through efficient utilization of time for model training across the tasks. Finally, in Fig. 6(b), we compare the overall execution time cost of our proposed method against the traditional synchronous aggregation rule (i.e., using synchronized aggregations for both edge and cloud/global model aggregations). When the global model of all tasks reaches the aforementioned desired accuracies, with 25 vehicles, our method reduces the average time cost by 15.57% across various training data samples;

while with 50 vehicles, it achieves a 10% reduction. These results underscore the notable time savings offered by our hybrid synchronous-asynchronous aggregation rule compared to conventional synchronous aggregation methods used in existing HFL and VEC-HFL methods [9], [19].

## VI. CONCLUSION AND FUTURE WORK

In this paper, we took one of the first steps towards addressing the challenges of unbalanced task scheduling, model obsolescence, and low data utilization in multi-model training within the vehicle-edge-cloud integrated hierarchical federated learning (VEC-HFL) architecture. We introduced a hybrid synchronous-asynchronous aggregation rule to guide the training process, combining the advantages of both synchronous and asynchronous methods. Building upon this rule, we proposed a novel methodology called the Hybrid Evolutionary And gReedy allocaTion method (HEART) to achieve balanced task scheduling and optimal task training prioritization. Extensive simulations on real-world datasets demonstrated that HEART significantly improves the efficiency of multi-model training, reducing the model training time and communication overhead compared to benchmark methods. For future work, extending our framework to incorporate additional factors within the VEC-HFL architecture is promising. This includes considering variable vehicle arrival and departures, fluctuating vehicular computing availability, data storage constraints at the vehicles, and the freshness and temporal variations of on-board datasets at vehicles. Additionally, addressing further uncertainties in the IoV environment, such as unexpected disconnections between vehicles and edge servers during model training, can be an interesting future direction.

## REFERENCES

- [1] W. Wu, M. Li, K. Qu, C. Zhou, X. Shen, W. Zhuang, X. Li, and W. Shi, “Split Learning Over Wireless Networks: Parallel design and resource management,” *IEEE J. Sel. Areas Commun.*, vol. 41, no. 4, pp. 1051–1066, 2023.
- [2] J. Cheng, G. Yuan, M. Zhou, S. Gao, C. Liu, H. Duan, and Q. Zeng, “Joint client selection and model compression for efficient fl in uav-assisted wireless networks,” *IEEE Trans. Veh. Technol.*, vol. 73, no. 10, pp. 15172–15184, 2024.
- [3] W. Hou, H. Wen, N. Zhang, W. Lei, H. Lin, Z. Han, and Q. Liu, “Adaptive training and aggregation for federated learning in multi-tier computing networks,” *IEEE Trans. Mobile. Comput.*, vol. 23, no. 5, pp. 4376–4388, 2024.
- [4] Z. Xu, D. Zhao, W. Liang, O. F. Rana, P. Zhou, M. Li, W. Xu, H. Li, and Q. Xia, “HierFedML: Aggregator placement and ue assignment for hierarchical federated learning in mobile edge computing,” *IEEE Trans. Parallel Distrib. Syst.*, vol. 34, no. 1, pp. 328–345, 2023.
- [5] Q. Wu, X. Chen, T. Ouyang, Z. Zhou, X. Zhang, S. Yang, and J. Zhang, “HiFlash: Communication-efficient hierarchical federated learning with adaptive staleness control and heterogeneity-aware client-edge association,” *IEEE Trans. Parallel Distrib. Syst.*, vol. 34, no. 5, pp. 1560–1579, 2023.
- [6] Z. Tang, X. Chu, R. Y. Ran, S. Lee, S. Shi, Y. Zhang, Y. Wang, A. Q. Liang, S. Avestimehr, and C. He, “Fedml Parrot: A scalable federated learning system via heterogeneity-aware scheduling on sequential and hierarchical training,” *arXiv preprint arXiv:2303.01778*, 2023.
- [7] Z. Dong, X. Zhu, J. Cao, Y. Jiang, V. K. Lau, and S. Sun, “Fuzzy logic assisted client selection and energy-efficient joint optimization for hierarchical federated learning,” *IEEE Int. Conf. Commun. (ICC)*, Rome, Italy, 2023, pp. 1262–1267.
- [8] B. Xie, Y. Sun, S. Zhou, Z. Niu, Y. Xu, J. Chen, and D. Gunduz, “MOB-FL: Mobility-aware federated learning for intelligent connected vehicles,” *IEEE Int. Conf. Commun. (ICC)*, Rome, Italy, 2023, pp. 3951–3957.
- [9] H. Zhou, Y. Zheng, H. Huang, J. Shu, and X. Jia, “Toward robust hierarchical federated learning in internet of vehicles,” *IEEE Trans. Intell. Transp. Syst.*, vol. 24, no. 5, pp. 5600–5614, 2023.

- [10] X. Kong, H. Gao, G. Shen, G. Duan, and S. K. Das, “FedVCP: A federated-learning-based cooperative positioning scheme for social internet of vehicles,” *IEEE Trans. Comput. Social Syst.*, vol. 9, no. 1, pp. 197–206, 2022.
- [11] Z. Wu, S. Sun, Y. Wang, M. Liu, Q. Pan, X. Jiang, and B. Gao, “FedICT: Federated multi-task distillation for multi-access edge computing,” *IEEE Trans. Parallel Distrib. Syst.*, vol. 35, no. 6, pp. 1107–1121, 2024.
- [12] Z. Chang, S. Hosseinalipour, and M. Chiang, “Asynchronous multi-model dynamic federated learning over wireless networks: Theory, modeling, and optimization,” *IEEE Trans. Cogn. Commun. Netw.*, vol. 10, no. 5, pp. 1989–2004, 2024.
- [13] H. Ma and H. Guo, “Communication-efficient federated multitask learning over wireless networks,” *IEEE Internet Things J.*, vol. 10, no. 1, pp. 609–624, 2023.
- [14] Z. Li, H. Wu, Y. Lu, B. Ai, Z. Zhong, and Y. Zhang, “Matching game for multi-task federated learning in internet of vehicles,” *IEEE Trans. Veh. Technol.*, vol. 73, no. 2, pp. 1623–1636, 2024.
- [15] X. Wei, J. Liu, and Y. Wang, “Joint participant selection and learning scheduling for multi-model federated edge learning,” *IEEE Int. Conf. Mobile Ad Hoc and Smart Syst. (MASS)*, Denver, CO, USA, 2022, pp. 537–545.
- [16] S. Luo, X. Chen, Q. Wu, Z. Zhou, and S. Yu, “HFEL: Joint edge association and resource allocation for cost-efficient hierarchical federated edge learning,” *IEEE Trans. Wireless Commun.*, vol. 19, p. 6535–6548, 2020.
- [17] P. Zhang, D. Tian, J. Zhou, X. Duan, Z. Sheng, D. Zhao, and D. Cao, “Joint optimization of platoon control and resource scheduling in cooperative vehicle-infrastructure system,” *IEEE Trans. Intell. Veh.*, vol. 8, no. 6, pp. 3629–3646, 2023.
- [18] L. Xu, Z. Zhang, Y. Yao, and Z. Yu, “Improved particle swarm optimization-based bp neural networks for aero-optical imaging deviation prediction,” *IEEE Access*, vol. 10, pp. 943–956, 2022.
- [19] T. Wang, X. Huang, Y. Wu, L. Qian, B. Lin, and Z. Su, “UAV swarm-assisted two-tier hierarchical federated learning,” *IEEE Trans. Netw. Sci. Eng.*, vol. 11, no. 1, pp. 943–956, 2024.
- [20] K.-I. Mahider, M. Ferfra, and R. Rabeh, “Optimization of statcom pi controller parameters using the hybrid ga-pso algorithm,” *IEEE Int. Conf. on Sys. and Cont. (ICSC)*, Sousse, Tunisia, 2023, pp. 270–275.
- [21] X. Yuan, H. Tian, W. Zhang, H. Zhao, Z. Zhao, and N. Zhang, “CAPSO: A combinatorial auction and improved particle swarm optimization based computation offloading approach for e-healthcare,” *IEEE Int. Conf. Commun. (ICC)*, Seoul, Korea, Republic of, 2022, pp. 3850–3855.
- [22] K. Zhuang, L. Xu, L. Li, L. Wang, and A. Fei, “GA-MADDPG: A demand-aware uav network adaptation method for joint communication and positioning in emergency scenarios,” *IEEE Wirel. Commun. and Net. Conf. (WCNC)*, Glasgow, United Kingdom, 2023, pp. 1–6.
- [23] Q. Wang and P. Du, “Accuracy assessment of industrial heritage mapping based on ga+bp neural networks forecast,” *IEEE Int. Conf. on Applied Int. and Sust. Comput. (ICAISC)*, Dharwad, India, 2023, pp. 1–5.
- [24] S. Karen and Z. Andrew, “Very deep convolutional networks for large-scale image recognition,” *arXiv preprint arXiv:1409.1556*, 2015.
- [25] K. He, X. Zhang, S. Ren, and J. Sun, “Deep residual learning for image recognition,” *arXiv preprint arXiv:1512.03385*, 2015.
- [26] B. V. Christian, K. Adrian, and S. B. Erling, “Long short-term memory rnn,” *arXiv preprint arXiv:2105.06756*, 2021.
- [27] H. Yang, J. Zhao, Z. Xiong, K.-Y. Lam, S. Sun, and L. Xiao, “Privacy-Preserving Federated Learning for UAV-Enabled Networks: Learning-based joint scheduling and resource management,” *IEEE J. Sel. Areas Commun.*, vol. 39, no. 10, pp. 3144–3159, 2021.
- [28] Y. Lu, C. Liu, F. Chang, H. Liu, and H. Huan, “JHPFA-Net: Joint head pose and facial action network for driver yawning detection across arbitrary poses in videos,” *IEEE Trans. Intell. Transp. Syst.*, vol. 24, no. 11, pp. 11850–11863, 2023.
- [29] S. Luo, X. Chen, Q. Wu, Z. Zhou, and S. Yu, “HFEL: Joint edge association and resource allocation for cost-efficient hierarchical federated edge learning,” *IEEE Trans. Wireless Commun.*, vol. 19, no. 10, pp. 6535–6548, 2020.
- [30] R. Khef, E. Driouch, and W. Ajib, “On the optimization of UAV-assisted wireless networks for hierarchical federated learning,” *IEEE Annual Int. Symp. Pers., Ind. Mobile Radio Commun. (PIMRC)*, Toronto, Canada, 2023, pp. 1–6.